

Accepted Manuscript

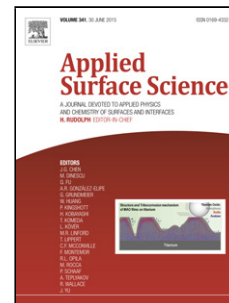
Title: Transparent conductive Hf-doped In₂O₃ thin films by RF sputtering technique at low temperature annealing

Author: G.H. Wang C.Y. Shi L. Zhao H.W. Diao W.J. Wang

PII: S0169-4332(16)32696-4
DOI: <http://dx.doi.org/doi:10.1016/j.apsusc.2016.11.239>
Reference: APSUSC 34544

To appear in: *APSUSC*

Received date: 23-8-2016
Revised date: 24-11-2016
Accepted date: 30-11-2016

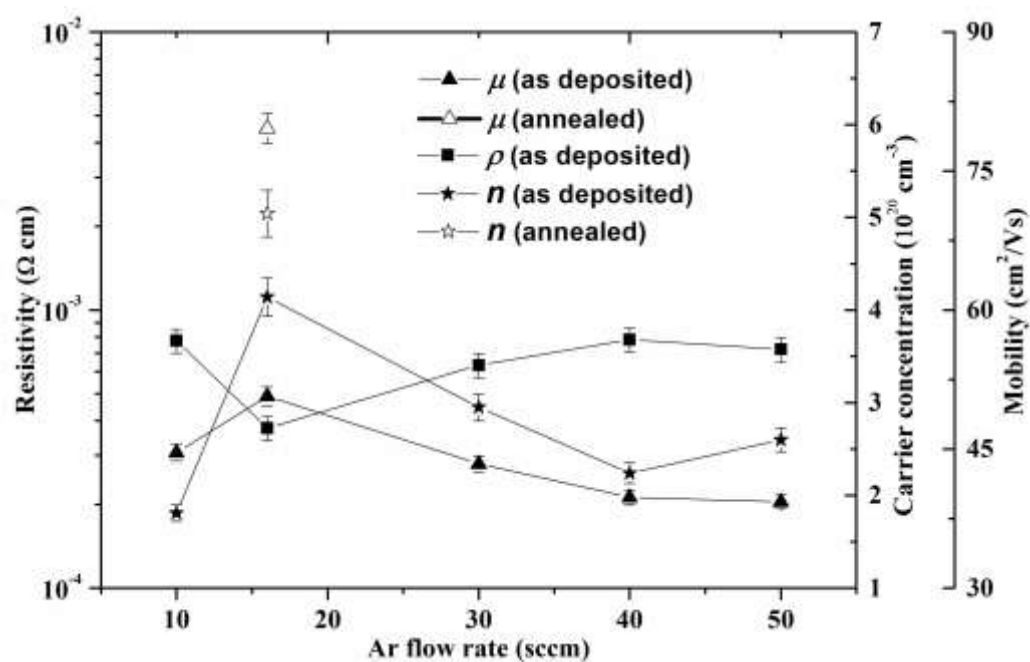


Please cite this article as: G.H.Wang, C.Y.Shi, L.Zhao, H.W.Diao, W.J.Wang, Transparent conductive Hf-doped In₂O₃ thin films by RF sputtering technique at low temperature annealing, *Applied Surface Science* <http://dx.doi.org/10.1016/j.apsusc.2016.11.239>

This is a PDF file of an unedited manuscript that has been accepted for publication. As a service to our customers we are providing this early version of the manuscript. The manuscript will undergo copyediting, typesetting, and review of the resulting proof before it is published in its final form. Please note that during the production process errors may be discovered which could affect the content, and all legal disclaimers that apply to the journal pertain.

Graphical abstract

High mobility IHFO film was prepared at a low substrate and thermal treatment temperature.



Highlights

Hf-doped In_2O_3 transparent conductive films (IHFO) were investigated by sputtering.

High mobility IHFO was prepared at a low substrate and thermal treatment temperature.

IHFO showed high transmittance with above 83% in the range of 300-1500 nm.

Optimized IHFO improved the efficiency of amorphous silicon germanium solar cell.

Transparent conductive Hf-doped In₂O₃ thin films by RF sputtering technique at low temperature annealing

G.H.Wang^a, C.Y. Shi^{b,*}, L.Zhao^a, H.W.Diao^a, W.J.Wang^a

^a*Key Laboratory of Solar Thermal Energy and Photovoltaic System of Chinese Academy of Sciences, Institute of Electrical Engineering, the Chinese Academy of Sciences, Beijing 100190, China*

^b*China Telecommunication Technology Labs, China Academy of Information and Communication Technology, Beijing 100015, China*

Abstract

Hf-doped In₂O₃ transparent conductive polycrystalline films (IHFO) were grown at a low substrate temperature by radio frequency magnetron sputtering for the applications of silicon-based solar cell. The effect of argon flow rate on the electrical and optical properties of the films was investigated. Low temperature thermal treatment improved IHFO films properties, with the optimal Hall mobility of 79.6 cm²/Vs and resistivity of 3.76×10⁻⁴ Ω cm. The average transmittance of the 807 nm thick IHFO films in the range of 300 - 1500 nm was above 83%. The carrier density was utilized to evaluate the plasma wavelength of IHFO conducting film which was 1.8 μm. The optimized IHFO film was then applied to amorphous silicon germanium thin film solar cells as the contacting layer. Compared to the cell without such a layer, the efficiency was higher by 0.35%.

Keywords Transparent conductive oxide films; Hf-doped In₂O₃; Radio frequency sputtering; Hall mobility; low temperature annealing

1. Introduction

Transparent conducting oxide films are of considerable interest in many

* Corresponding author. Tel.: +86 10 82547043; fax: +86 10 82547041
E-mail address: shichengying@caict.ac.cn (C.Y. Shi)

optoelectronic applications such as optical detectors, solar cells and flat-panel displays [1-5]. Employing high mobility (μ) films as electrodes for thin film solar cells is promising for efficiency improvement. Many TCO film with high μ were obtained at either high deposition temperatures or with high-temperature post-thermal treatments, which limited their application to a-Si/c-Si heterojunction (SHJ) or other thin film solar cells fabricated at low temperature [6-9]. Metal-doped In_2O_3 thin film prepared by different method to obtain high mobility has attracted considerable attention. Recently, Meng *et al.* obtained a maximum μ of $89 \text{ cm}^2/\text{Vs}$ for $\text{In}_2\text{O}_3:\text{W}$ (IWO) films at lower than 200°C substrate temperature by reactive plasma deposition (RPD) technique. Consequently, a conversion efficiency of 20.8% was obtained by applying the film to the SHJ solar cell [10]. Kobayashi *et al.* reported CeO_2 -doped hydrogenated In_2O_3 (ICO:H) films deposited by high-density plasma-enhanced evaporation (HPE) with superior μ values of $141 \text{ cm}^2/\text{Vs}$. In addition, H-doped In_2O_3 (IO:H) films also showed high μ exceeding $105 \text{ cm}^2/\text{Vs}$ [11,12]. In most of the aforementioned literature, oxygen was used as a reactive precursor to improve the TCO film properties. However, oxygen usage during deposition complicates the process. So far, there were only very few reports on the μ and transmittance data of Hf-doped In_2O_3 transparent conductive films (IHFO) deposited by magnetron sputtering without oxygen at low substrate temperature.

In this work, the optical, structural and electrical properties of IHFO films were simultaneously investigated for the applications of amorphous silicon germanium (a-SiGe) solar cells, in which it serves as the conductive layer on the rear surface. This

study also aims at the reduction of mass production complexity by excluding oxygen as a variable parameter.

2. Experimental details

The IHFO films were deposited on quartz or polished silicon substrates by radio frequency magnetron sputtering from a sintered ceramic HfO₂-doped In₂O₃ (1 wt.%) target in an argon atmosphere. The films were deposited using various argon (Ar) flow rates from 10 to 50 sccm at a substrate of 150 °C. The thickness of the films was measured by a Veeco Dektak 200 surface profiler. The crystalline structures of films were monitored by X-ray diffractometer (XRD) using a Cu-K α irradiation source. Scanning electron microscopy (SEM) (ZEISS SIGMA) was used to characterize the surface and cross-sectional images. The hafnium (Hf) content in IHFO films was analyzed by EDX on the SEM at high voltage of 15.0 kv. The surface morphology and roughness was checked by an atomic force microscopy (AFM) (Bruker Model Icon). The optical reflection and transmittance was measured by a Varian Excalibur HE 3100 UV-VIS-NIR Spectrophotometer. The electrical properties of the IHFO films were analyzed by Hall effect measurement system HL 5500 PC (Nanometrics).

The a-Si and a-SiGe thin films were fabricated in a capacitively coupled radio frequency plasma enhanced chemical vapor deposition (RF-PECVD) system with a base vacuum of 10⁻⁵ Pa. The reactive gases for the deposition were silane (SiH₄), Germane (GeH₄), hydrogen (H₂), diborane (B₂H₆) and phosphine (PH₃). The pressure and flow rates were independently varied by a downstream throttle valve controller and upstream mass flow controllers, respectively. The photo current-density versus

voltage (J-V) characteristics of the fabricated solar cells was measured at 25 °C under 1-sun (AM1.5, 100 mW/cm²) solar simulator radiation.

3. Results and discussion

Fig.1 shows the XRD patterns of the IHFO films deposited at 10, 16, 30, 40 and 50 sccm Ar flow rates. The thickness of all IHFO films is about 490 ± 30 nm. The films show typical polycrystalline structures with the weak diffraction peaks of (122), (222), (400), (411), (431), (440) and (622) together. The structure is dominated by a strong (222) peak near 30.2° under low Ar flow rates. Its intensity decreases with the Ar flow rate, while other peaks intensify. There is a large increment in the (400) peak intensity at 35°, which corresponds to In₂O₃ with a preferred [100] orientation. It shows that an increment in Ar flow rate favours the preferred orientation along the (400) direction. For ITO films sputtered in pure argon, the preferential orientation along the [100] orientation is always more pronounced at higher RF power [13, 14], since higher RF power enhances the mobile energy of sputtered atoms on substrates and hence improves the crystallinity of ITO films. However, for IHFO films deposited at constant RF power, oxygen vacancies concentration might play a role in changing the preferred orientations from (222) to (400) with the Ar flow rate [15-19]. The low concentration of oxygen vacancies leads to more favour to the (111) textured IHFO growth at low Ar flow rate. Moreover, because the high atomic density (111) plane present a lower surface free energy than the (001) planes, the (111) texture should be preferentially observed. When concentration of oxygen vacancies will increase with Ar flow rate, (001) textured IHFO growth is dominant. The growth under high Ar

flow rate will lead to In-rich conditions favouring the (001) textured IHFO growth. The incident indium species reach the substrate surface. Such In species will play a key role by acting as an auto surfactant that lowers the surface free energy difference between the (001) and (111) surface [20, 21].

The crystal sizes of the films are calculated using the Scherrer equation (1) from XRD spectra [22]

$$D_{hkl} = 0.89 \frac{\lambda}{\beta \cos \theta} \quad (1)$$

Where D_{hkl} is the crystal size; λ is the X-ray wavelength, β is the FWHM of each peak as a function of 2θ . Furthermore, θ is the Bragg angle. Fig.2 shows the average crystal sizes of the films calculated using the Scherrer equation from XRD spectra. The crystal size becomes larger with the Ar flow rate, which shows an increment of the film crystallinity. When the crystallinities are low, the grain boundary scattering was dominant. However, thin films are highly crystallized and the ionized impurity scattering is dominant. The ionized impurity scattering might be dominant with the Ar flow rate [23].

Fig.3 shows the SEM images of an IHFO film on polished Si substrate. The thickness is about 807 nm. The film is deposited uniformly on the Si substrate. A dense granular structure can be observed in the surface scan, while columnar structures perpendicular to the Si substrate is shown in the cross-sectional image. The well crystallized IHFO film agrees with the XRD analysis.

Fig.4 shows the resistivity (ρ), carrier concentration (n) and μ of the IHFO films as a function of Ar flow rate. It is clear that electrical properties are sensitive to Ar

flow rate. The ρ increases from a minimum value of $3.74 \times 10^{-4} \Omega \text{ cm}$ at 16 sccm to $7.84 \times 10^{-4} \Omega \text{ cm}$, while the μ and n reaches the $50.7 \text{ cm}^2/\text{Vs}$ and $4.41 \times 10^{20} \text{ cm}^{-3}$ respectively at 16 sccm Ar flow rate, and then decreases markedly with the Ar flow rate. The films crystallinity increment does not improve the μ because of smaller grain scattering with the Ar flow rate. IHFO film is an n-type semiconductor. The increment of ionized impurity scattering probably originated from oxygen vacancies might play a role in determining the mobility decrement [24]. The n increases and ρ decreases at low Ar flow rate when the concentration of oxygen vacancies acting as electron donors improves. The concentration of oxygen vacancies will further improve with increasing Ar flow rate, and such vacancies will be close together. This fact might induce the phenomenon of annihilation of oxygen vacancies, which will lead to the creation of neutral In and a decrement in the n , and it follows that the ρ will increase with the Ar flow rate [25].

The Hf content in the film by EDX before annealing reaches the 2.82 ± 0.64 Wt. %, which is higher than the one of target. It is deduced that Hf substitutes probably for In site in the indium oxide lattice, furthermore, the incorporation of Hf with O will form the Hf-O complex [10, 26].

The annealing plays a dominant role in governing the film growth mechanism which determines the film microstructure and properties. The optimal sample obtained at 16 sccm Ar flow rate is annealed for 2 hours in air at 230°C . Fig.4 shows the low temperature annealing process increases μ from 50.7 to $79.6 \text{ cm}^2/\text{Vs}$ and n from $4.14 \times 10^{20} \text{ cm}^{-3}$ to $5.04 \times 10^{20} \text{ cm}^{-3}$ at 16 sccm Ar flow rate.

Meng *et al.* have attributed a higher μ to a higher oxygen partial pressure [10]. In this work, oxygen is not introduced in the sputtering process. Nevertheless, the annealing process in air might reduce the number of oxygen vacancies in the films, which led to a higher μ [27]. Fig.5 shows the roughness of different thickness films before ((a) and (b)) and after ((a') and (b')) annealing. The film thickness in (a) and (b) is 436 nm and 807 nm, respectively. The insets of figure are surface morphologies of different thickness films before and after annealing. The root mean square (R_q) of the surface roughness decreases after annealing for both films. The clusters of grain for 436 nm thick film are presented and grains become denser with size increment from 110 ± 10 to 130 ± 10 nm for 807 nm one after the thermal treatment, which leads to less grain boundaries that behave as traps for free carries and barriers for their transport in the films. Hence, less grain boundary scattering leads to a μ improvement. Many carriers were probably released from the crystallized area. These facts imply that the dopant Hf must be inactive in the amorphous IHFO and become active with raised crystallization during annealing, as reported in some studies [28, 29]. So n increased after annealing.

Optical transmittance is considered as one of the most essential properties in evaluating the optical performance of TCO film. Fig.6 shows the transmittance and reflectance spectra of 807 nm thick IHFO film deposited at 16 sccm Ar flow rate. The inset shows Tauc plot from which the optical band gap (E_g) value of IHFO film is determined. The average transmittance in the range of 300 - 1500 nm is above 83% and reaches 90% at 550 nm wavelength.

The high μ in TCO film means a larger wavelength transparency limit, which is characterized by the plasma wavelength λ_p . λ_p can be calculated according to the Drude model [10, 30-32]

$$\lambda_p = 2\pi c \left(\frac{\epsilon_0 \epsilon_\infty m_c^*}{n e^2} \right)^{1/2} \quad (2)$$

Where c is the velocity of light, n is the carrier density, e is the electronic charge, ϵ_0 is the permittivity of free space, ϵ_∞ is the high frequency permittivity, m_c^* is the conductivity effective mass, ϵ_∞ and m_c^* are assumed as 4 and 0.3 m_e , respectively. λ_p of the IHFO film deposited at 16 sccm Ar flow rate is then calculated as 1.8 μm . The larger λ_p therefore extends the transparency window into the NIR region.

Based on the transmittance and reflectance data of IHFO films, the E_g calculated is 3.43 eV by Tauc's equation (3) [33]

$$(\alpha h\nu)^{1/2} = B(h\nu - E_g) \quad (3)$$

Where $h\nu$ is the photon energy, B is a constant, α is the absorption coefficient, so that E_g is obtained by extrapolation of the linear fit to $\alpha=0$.

The absorption coefficient is estimated by the following formula (4)

$$\alpha = \frac{\ln\left(\frac{(1-R)^2}{T}\right)}{d} \quad (4)$$

Where α is the absorption coefficient, d is the thickness of thin film, R and T is the optical reflection and transmission of thin film, respectively.

The a-SiGe thin film solar cell has been widely investigated for photovoltaic power generation, because of their narrow band gap for use in tandem and triple junction solar cells. At device level, an IHFO film is applied to a-SiGe solar cells as

the contact layer. The thickness of the IHFO film is about 80 nm. Fig.7 shows the performance of the a-SiGe solar cell. The inset of figure is the a-SiGe solar cell schematic diagram in this work. The solar cells are fabricated with the structure of glass/textured SnO₂:F/p-i-n a-SiGe/IHFO/Al. The thickness of a-SiGe layer is 150 nm. It can be observed that, compared to the reference cell without such a contact layer, the efficiency increases by 0.35% by inserting an IHFO layer, mainly due to an increment in the short-circuit current density (J_{sc}). In addition, the V_{oc} also reaches to 0.79 V.

The external quantum efficiency (EQE) curves of the solar cells with and without IHFO contact layers are shown in Fig.8. Clearly, EQE of the solar cell with IHFO contact layer dramatically intensifies in the 550 - 800 nm range compared to the reference. The solar cell performance thus improves to a great extent, in which IHFO film between n-layer and Al back reflector is an effective diffusion barrier to reduce the diffusion of Al atoms into the absorber film of solar cell [34].

4 Conclusion

In this study, the structural, electrical and optical properties of the IHFO films fabricated by intermediate frequency magnetron sputtering were investigated. XRD study on the films showed typical polycrystalline structures. The cross-sectional SEM image showed columnar structures perpendicular to the substrate. The film ρ initially reduced from $7.76 \times 10^{-4} \Omega \text{ cm}$ to $3.76 \times 10^{-4} \Omega \text{ cm}$ at 16 sccm with the Ar flow rate, followed by a sharp increment to $7.84 \times 10^{-4} \Omega \text{ cm}$. Low temperature thermal annealing increased the grain size and grain clusters of the IHFO films, resulting in an improved

μ and n . Similarly, μ reached to the maximum value of 79.6 cm²/Vs at the same flow rate. The average transmittance of an 807 nm thick IHFO film in the range of 300 - 1500 nm was above 83%. Finally, an 80 nm thick film was applied to a-SiGe solar cell as a contact layer. The inclusion of such a layer boosted the EQE in the 550 - 800 nm range, which translated to an improvement of efficiency of 0.35%. This is mainly attributed to an increment in the J_{sc} of the solar cells.

Acknowledgments

The authors gratefully acknowledge Dr. Jia Ge for revision and discussion. The work is supported by the National Natural Science Foundation of China (62004200 and 61274061) and the Chinese Scholarship Council (201504910179).

References

- [1] D. S. Ginley, C. Bright, Transparent conducting oxides, MRS Bulletin 25 (2000) 15-18.
- [2] K. L. Chopra, S. Major, D. K. Pandya, Transparent conductors - a status review, Thin Solid Films 102 (1983) 1-46.
- [3] Y. J. Lee, H. Park, M. Ju, Y. Kim, J. Park, D. V. Ai, S. Q. Hussain, Y. Lee, S. Ahn, J. Yi, Improvement of haze ratio of DC (direct current)-sputtered ZnO:Al thin films through HF (hydrofluoric acid) vapor texturing, Energy 66 (2014) 20-24.
- [4] A. Solieman, M. A. Aegerter, Modeling of optical and electrical properties of In₂O₃:Sn coatings made by various techniques, Thin Solid Films 502 (2006) 205-211.
- [5] J. H. Shin, J. S. Lee, C. S. Hwang, S. H. KoPark, W. S. Cheong, M. K. Ryu, C. W.

Byun, J. I. Lee, H. Y. Chu, Light effects on the bias stability of transparent ZnO thin film transistors, ETRI Journal 31 (2009) 62-64.

[6] D. Zhang, A. Tavakoliyaraki, Y. Wu, R. A. C. M. M. van Swaaij, M. Zeman, Influence of ITO deposition and post annealing on HIT solar cell structures, Energy Procedia 8 (2011) 207-213.

[7] T. Koida, M. Kondo, High-mobility transparent conductive Zr-doped In_2O_3 , Applied Physics Letter 89 (2006) 082104-1-3.

[8] R. Hashimoto, Y. Abe, T. Nakada, High mobility titanium-doped In_2O_3 , thin films prepared by sputtering/post-annealing technique, Applied Physics Express 1 (2008) 015002-1-3.

[9] R. K. Gupta, K. Ghosh, S. R. Mishra, P. K. Kahol, High mobility Ti-doped In_2O_3 transparent conductive thin films, Materials Letters 62 (2008) 1033-1035.

[10] F. Y. Meng, J. H. Shi, Z. X. Liu, Y. F. Cui, Z. D. Lu, Z. Q. Feng, High mobility transparent conductive W-doped In_2O_3 , thin films prepared at low substrate temperature and its application to solar cells, Solar Energy Materials and Solar Cells 122 (2014) 70-74.

[11] E. Kobayashi, Y. Watabe, T. Yamamoto, Y. Yamada, Cerium oxide and hydrogen co-doped indium oxide films for high-efficiency silicon heterojunction solar cells, Solar Energy Materials & Solar Cells 149 (2016) 75-80.

[12] E. Kobayashi, Y. Watabe, T. Yamamoto, High-mobility transparent conductive thin films of cerium-doped hydrogenated indium oxide, Applied Physics Express 8 (2015) 015505-1-4.

- [13] S. Q. Hussain, W.-K. Oh, S. Ahn, A. H. T. Le, S. Kim, S. M. Iftiqar, S. Velumani, Y. Lee, J. Yi, Highly transparent RF magnetron-sputtered indium tin oxide films for a-Si:H/c-Si heterojunction solar cells amorphous/crystalline silicon, *Materials Science in Semiconductor Processing* 24 (2014) 225-230.
- [14] E. Terzini, P. Thilakan, C. Minarini, Properties of ITO thin films deposited by RF magnetron sputtering at elevated substrate temperature, *Materials Science and Engineering: B* 77 (2000) 110-114.
- [15] O. Tuna, Y. Selamet, G. Aygun, L. Ozyuzer, High quality ITO thin films grown by dc and RF sputtering without oxygen, *Journal of Physics D: Applied Physics* 43 (2010) 055402-1-7.
- [16] M. Gulen, G. Yildirim, S. Bal, A. Varilci, I. Belenli, M. Oz, Role of annealing temperature on microstructural and electro-optical properties of ITO films produced by sputtering, *Journal of Materials Science: Materials in Electronics* 24(2) (2013) 467-474.
- [17] D. Kim, Y. Han, J.-S. Cho, S.-K. Koh, Low temperature deposition of ITO thin films by ion beam sputtering, *Thin Solid Films* 377-378 (2000) 81-86.
- [18] Seung-Ik Jun, T. E. McKnight, M. L. Simpson, P. D. Rack, A statistical parameter study of indium tin oxide thin films deposited by radio-frequency sputtering, *Thin Solid Films* 476 (2005) 59-64.
- [19] S. Venkatachalam, H. Nanjo, F. M. B. Hassan, K. Kawasaki, M. Kanakubo, T. Aizawa, T. Aida, T. Ebina, Characterization of nanocrystalline indium tin oxide thin films prepared by ion beam sputter deposition method, *Thin Solid Films* 518 (2010)

6891-6896.

[20] M. Nistor, W. Seiler, C. Hebert, E. Mater, J. Perrière, Effects of substrate and ambient gas on epitaxial growth indium oxide thin films, *Applied Surface Science* 307 (2014) 455-460.

[21] W. Seiler, M. Nistor, C. Hebert, J. Perrière, Epitaxial undoped indium oxide thin films: Structural and physical properties, *Solar Energy Materials & Solar Cells* 116 (2013) 34-42.

[22] B.D. Cullity, *Elements of X-ray Diffraction*, Addison-Wesley, New York, 1978.

[23] Ho-Chul Lee, O. Ok Park, Electron scattering mechanisms in indium-tin-oxide thin films: grain boundary and ionized impurity scattering, *Vacuum* 75 (2004) 275-282.

[24] C. Guillén, J. Herrero, Structure, optical, and electrical properties of indium tin oxide thin films prepared by sputtering at room temperature and annealed in air or nitrogen, *Journal of Applied Physics* 101 (2007) 073514-1-7.

[25] E. Millon, M. Nistor, C. Hebert, Y. Davila, J. Perrière, Phase separation in nanocomposite indium tin oxide thin films grown at room temperature: on the role of oxygen deficiency, *Journal of Materials Chemistry* 22 (2012) 12179-12185.

[26] Z. D. Lu, F. Y. Meng, Y. F. Cui, J. H. Shi, Z. Q. Feng, Z. X. Liu, High quality of IWO films prepared at room temperature by reactive plasma deposition for photovoltaic devices, *Journal of Physics D: Applied Physics* 46 (2013) 075103-1-5.

[27] R. K. Gupta, K. Ghosh, S. R. Mishra, P. K. Kahol, High mobility W-doped In_2O_3 thin films: Effect of growth temperature and oxygen pressure on structural, electrical

and optical properties, *Applied Surface Science* 254 (2008) 1661-1665.

[28] H. Morikawa, M. Fujita, Crystallization and decrease in resistivity on heat treatment of amorphous indium tin oxide thin films prepared by d.c. magnetron sputtering, *Thin Solid Films* 339 (1999) 309-313.

[29] C. H. Yang, S. C. Lee, S. C. Chen, T. C. Lin, The effect of annealing treatment on microstructure and properties of indium tin oxides films, *Materials Science and Engineering B* 129 (2006) 154-160.

[30] I. Hamberg, C. G. Granqvist, Evaporated Sn-doped In_2O_3 films: basic optical properties and applications to energy-efficient windows, *Journal of Applied Physics* 60 (1986) R123-R159.

[31] T. J. Coutts, D. L. Young, X. N. Li, Characterization of transparent conducting oxides, *MRS Bulletin* 25 (2000) 58-65.

[32] I. A. Rauf, Extraction of free carrier density and mobility from the optical transmission data of tin-doped indium oxide thin films, *Materials Letters* 23 (1995) 73-78.

[33] J. Tauc, A. Menth, States in the gap, *Journal of Non-Crystalline Solids* 8-10 (1972) 569-585.

[34] G. H. Wang, L. Zhao, H. W. Diao, W. J. Wang, Optical enhancement by back reflector with $\text{ZnO}:\text{Al}_2\text{O}_3$ (AZO) of NiCr diffusion barrier for amorphous silicon germanium thin film solar cells, *Vacuum* 89 (2013) 40-42.

Figure Captions:

Fig.1 XRD spectra of IHFO films deposited at different Ar flow rate

Fig.2 Crystal sizes of the films calculated using the Scherrer equation from XRD spectra

Fig.3 (a) surface and (b) cross-sectional SEM images of an 807 nm thick IHFO film uniformly deposited on a polished Si substrate

Fig.4 ρ , n , μ of IHFO films as functions of Ar flow rate and n , μ of IHFO film deposited at 16 sccm Ar flow rate after annealing

Fig.5 The roughness of different thickness films before ((a) and (b)) and after ((a') and (b')) annealing. Film (a) is 436 nm thick and film (b) is 807 nm thick. The insets of figure are surface morphologies of corresponding films before and after annealing

Fig.6 The transmittance and reflectance spectra of 807 nm thick IHFO film deposited at 16 sccm Ar flow rate. The inset is Tauc plot from which the E_g value of IHFO film is determined.

Fig.7 J-V curves and performance parameters of a-SiGe solar cells with and without IHFO contact layer, the inset of figure is the a-SiGe solar cell schematic diagram in this work

Fig.8 EQE curves of a-SiGe solar cells with and without IHFO contact layer

Fig.1.

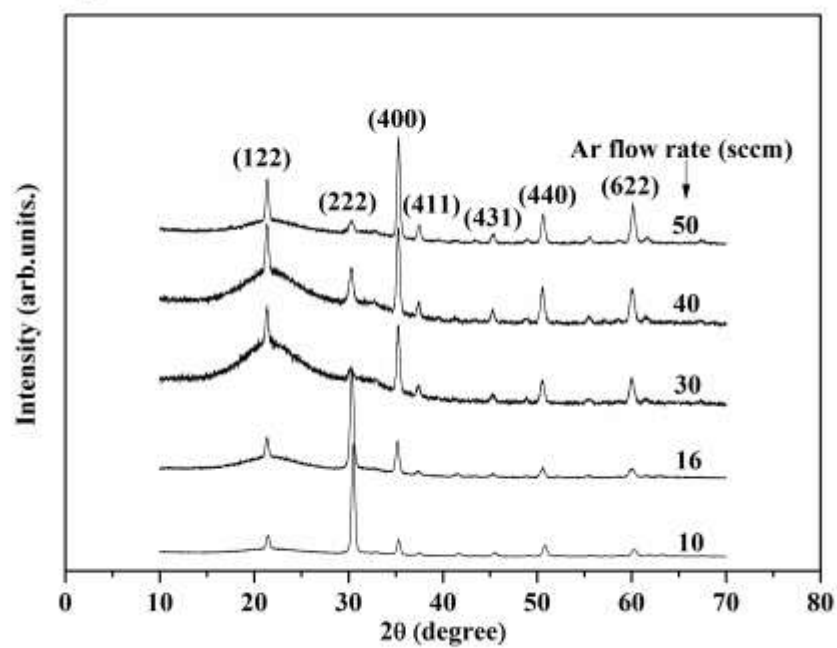


Fig.2.

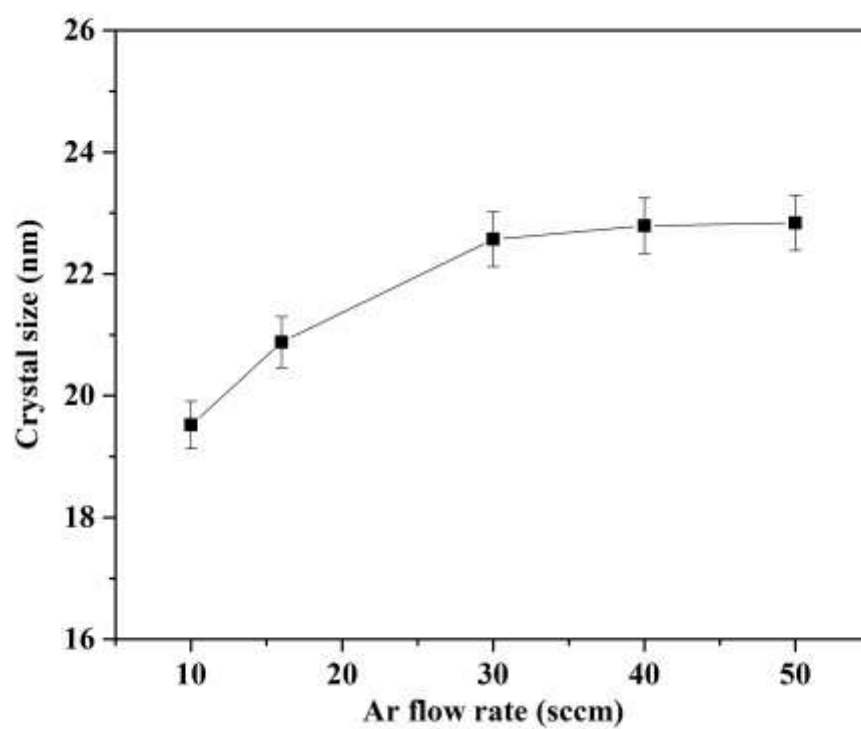


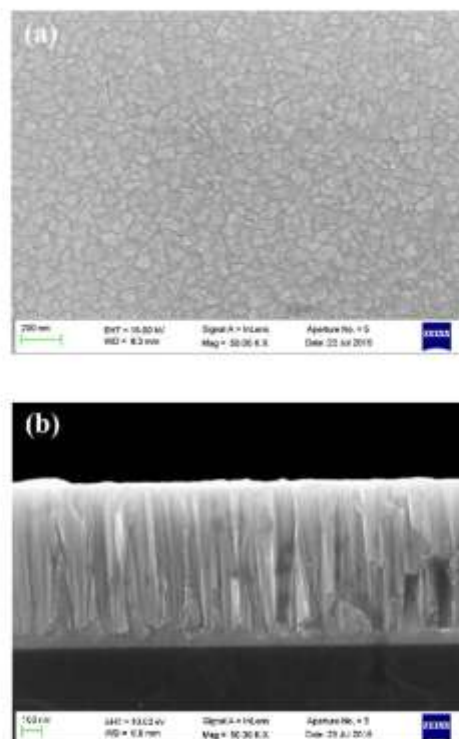
Fig.3.

Fig.4.

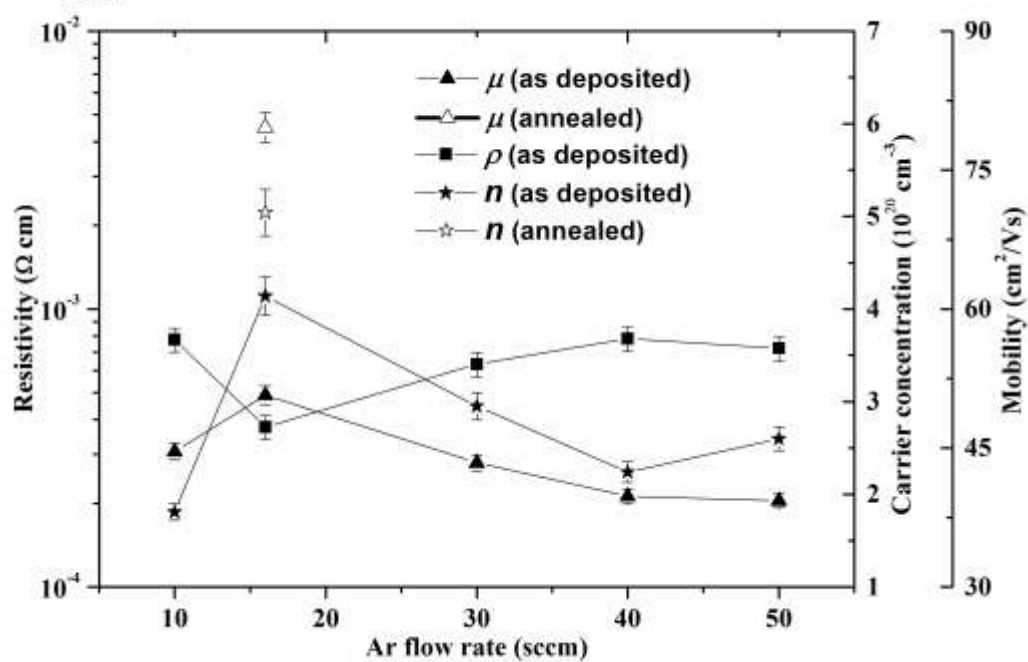


Fig.5.

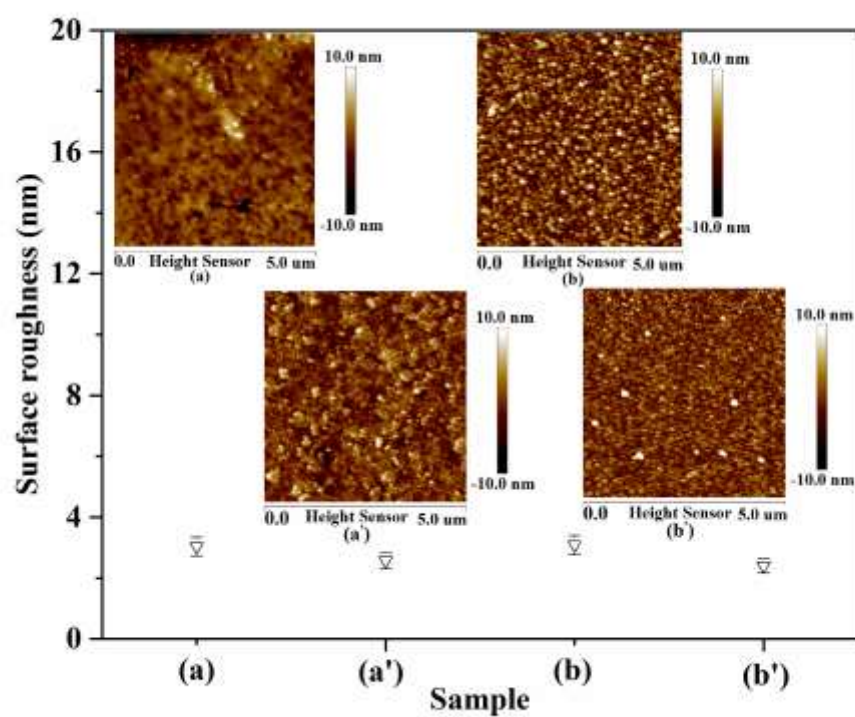


Fig.6.

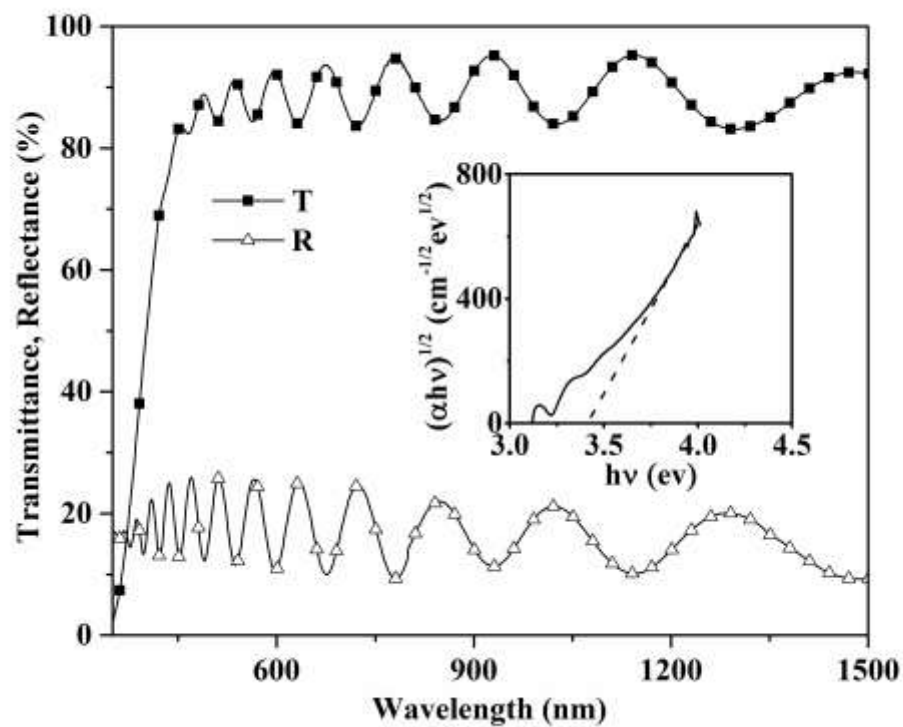


Fig.7.

